LBL-16890
UC-34a

Lawrence Berkeley Laboratory
UNIVERSITY OF CALIFORNIA

Accelerator & Fusion
Research Division

SPOT HEATING CALCULATION FOR A HEAVY ION DRIVEN HIGH TEMPERATURE EXPERIMENT

E.P. Lee and J. W-K. Mark

April 1984

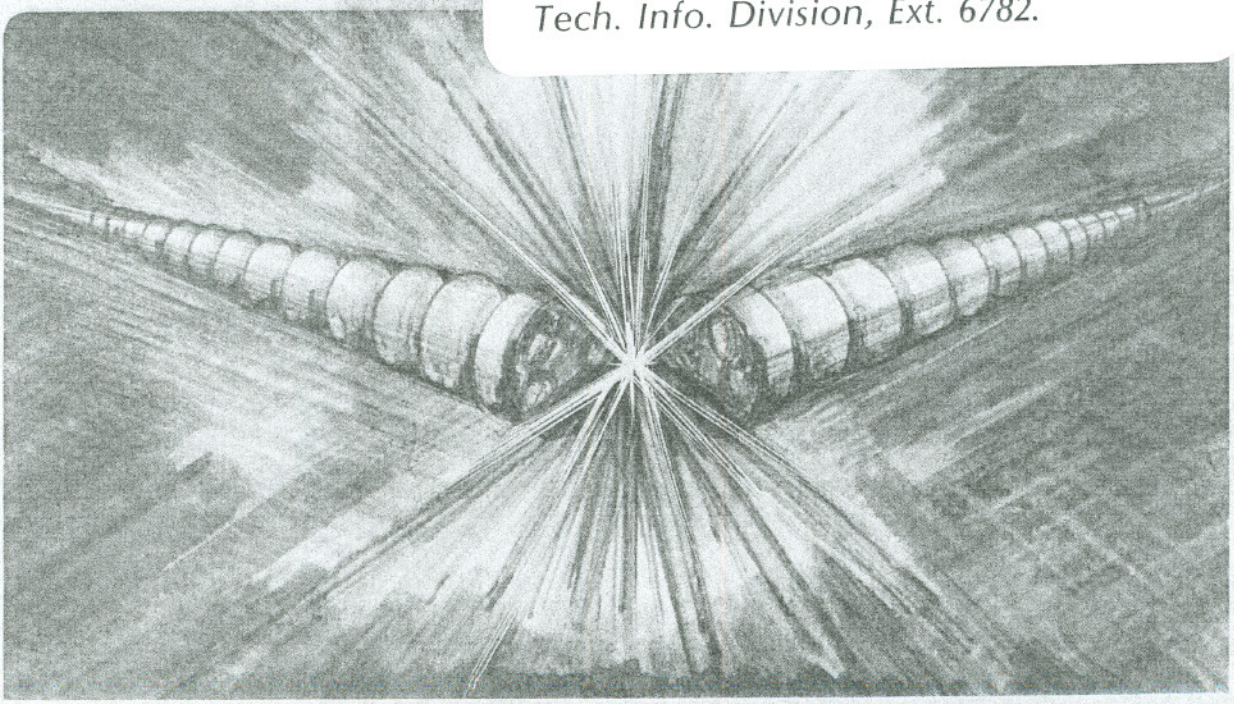

Prepared for the U.S. Department of Energy under Contract DE-AC03-76SF00098

HIFAN-226
LBL-16890

SPOT HEATING CALCULATION FOR A HEAVY ION DRIVEN HIGH TEMPERATURE EXPERIMENT*

Edward P. Lee and J. W-K. Mark

Accelerator and Fusion Research Division
Lawrence Berkeley Laboratory
University of California
Berkeley, CA 94720

April 1984

*This work was supported by the Office of Energy Research, Office of Basic Energy Sciences, Department of Energy under Contract No. DE-AC03-76SF00098.

HIFAN-226
LBL-16890

SPOT HEATING CALCULATION FOR A HEAVY ION DRIVEN HIGH TEMPERATURE EXPERIMENT*

Edward P. Lee and J. W-K. Mark†
Lawrence Berkeley Laboratory
University of California
Berkeley, CA 94720

Major Contributors: R.O. Bangerter and R. Kopp, Los Alamos Nat'l Laboratory

Abstract

An analytical model is used to predict the temperature reached in a spot heating experiment driven by a heavy ion beam. A discussion of physical processes and approximations is included.

I. Spot Heating with HTE

The High Temperature Experiment[1,2] (HTE) is needed to establish an adequate data base before one can proceed with confidence to a larger-scale application of accelerator technology to Inertial Confinement Fusion. Although HTE is primarily considered to be the focal point for development of the high current heavy ion accelerator technology, it is also intended to test several other important aspects of ICF specific to ion drivers. Three general categories of concern are addressed:

*This work was supported by the Office of Energy Research, Office of Basic Energy Sciences, Department of Energy under Contract No. DE-AC03-76SF00098.

†Lawrence Livermore Nat'l Laboratory, University of California, Livermore, CA 94550.

1. The handling of high ion currents during acceleration, bunching and final focus.

2. Final transport to the target: neutralization, stability, spot size, multi-beam interaction.

3. Material interaction: depositional anomalies, hot electron generation (if any), stability in the plasma plume, target charge-up.

Questions related to pellet and reactor chamber design are considered to be nearly decoupled from driver type, and are not addressed by HTE.

Simple spot heating experiments are considered adequate to address the issues of material interaction. A target[3] might be arranged as shown in Fig. 1. Roughly speaking, the goal is to raise a solid density target to temperatures of 50-100 eV using an accelerator driver type which can be extrapolated to reactor level parameters. This temperature range is considered sufficient to test material interaction characteristics, e.g., to discover any unknown difficulty associated with heavy ions. The target material need not be solid in the usual bulk sense -- felted Al of $\leq$ 1/10 normal density has been assumed[3] in order to obtain an adequate depth of ion penetration. The ions can have mass number considerably below the usual A = 200 assumed for a reactor driver and still be regarded as an adequate simulation; the most studied HTE choice has been 100-150 MeV Na^+ (A = 23). A Pb tamper is placed around the felted metal target to reduce losses by radial expansion. Longitudinal expansion is limited during the period of heating if the target depth is made sufficiently great by felting.

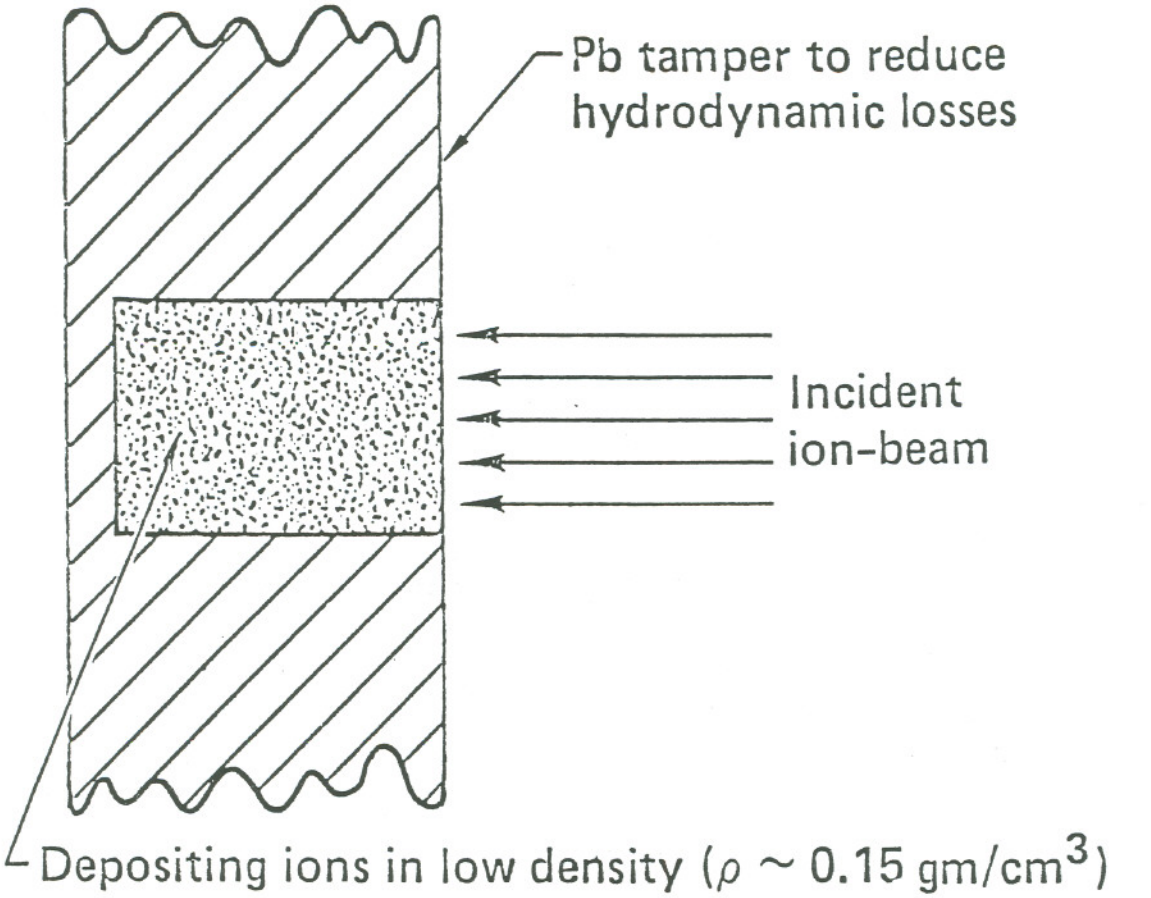

Figure 1. Spot heating disk target

The present report is intended to provide the HTE design study with a convenient calculation of spot heating temperatures. It is based on a simple model that includes only particle range, beam irradiance, radiation loss, and specific energy of the target material. A hydrodynamic disassembly scale time is estimated.

II. The Heating Equation

The temperature rise is evaluated by solving the rate equation[1,3]

$$\frac{d\varepsilon}{dt} = \frac{S - \sigma T^4}{R} , \tag{1}$$

where

$\varepsilon(T)$ = specific energy of target $\left(\frac{J}{gm}\right)$,

$S(t)$ = irradiance by beam $\left(\frac{watt}{cm^2}\right)$,

R = range of ions $\left(\frac{gm}{cm^2}\right)$,

σ = Stefan-Boltzmann constant = $1.028 \times 10^5 \left(\frac{watts}{cm^2\ eV^4}\right)$,

t = time (s),

T = temperature (eV).

The mathematical difficulties encountered in solving Eq. (1) arise from the dependence of S on time, which destroys separability, and the complex dependence of ε on temperature. In general a numerical treatment is

needed. However, approximations adequate for most situations of interest are introduced (Section VI) which evade these difficulties and yield a simple solution in tabular form.

The remaining tasks are to provide data for R and $\varepsilon(T)$, to solve Eq. (1), and to tabulate results for typical pulse parameters; these are carried out in Sections IV-VII. In Section III a short discussion of the physical assumptions underlying the model is provided.

III. Discussion of Heating Equation

(a) Point Model

Equation (1) has only time as an independent variable (point model), but a real target is finite in all dimensions. Ideally a 3-D code such as LASNEX[3] is used to resolve the complex interaction of beam and target, however it is an expensive and not generally available tool, and it is not well suited for fast surveys. Several bench mark (LASNEX) calculations for the HTE target geometry of Fig. 1 have been reported by Mark,[3] and results from the point model can be compared with them. This is done in Section VIII for a case of very high irradiance ($T > 200$ eV) which was reported in sufficient detail. A second (and new) comparison with LASNEX results is also given which uses parameters considered typical of HTE design. A surprisingly good agreement of calculated temperatures (~ 20%) found in the early stage of irradiance is attributed to the low degree of hydrodynamic response and radiation transport. Initially, simple heating takes place and this is well represented by a point model except for the spatial dependence of energy deposition. At intermediate times the strongly temperature dependent radiation loss rate ($\sim T^4$) tends to clamp T at a value which is insensitive to geometric details. At late times hydrodynamic expansion

causes T to drop -- this is not contained in the point model. The temperature predicted by the point model is expected to be most accurate near the beam axis since real beams have rounded profiles.

Geometric effects not included in the point model:

(1) Longitudinal expansion at late times (time scale is estimated);

(2) Radial expansion resulting from rounded beam profile;

(3) Bragg peak induced effects;

(4) Longitudinal convergence of irradiation due to converging approach angles of multiple beamlets.

(5) Radiation diffusion into the Pb tamper.

Further terms may be added to the point model [Eq.(1)] to take into account the bulk kinetic energy of the target and sideways diffusion of energy into the high-Z material. A simple code is then used to obtain numerical results. For typical HTE examples, the point model results are not significantly altered by these additional terms if pulse duration is not long compared with the estimated disassembly time.

(b) Radiation Transport

Radiation loss in the point model is approximated by the Stefan-Boltzmann law for surface emission. In reality there must be radiation transport from the target interior (which is at a higher temperature), and emission from a surface layer. The assumption of surface emission and constant interior temperature is crudely valid if the particle range equals the

optical depth. There is no way of assuring this to be the case in general, and it is expected that the target will be optically thick for the cases of current interest. Further calculations made with LASNEX seem called for here. If the optical depth is greater than the particle range, cooling will be more rapid than assumed. If the optical depth is shorter than the range the deep interior of the target will reach a higher temperature than predicted, but it will not be readily observable. In this case the observed temperature is characteristic of that at about one optical depth and should be slightly lower than that given by the point model.[3]

(c) Thermal Conduction

This mode of cooling and transport is estimated to be small, with a characteristic time on the order of several μs. The dominant carriers of heat are the copious free electrons, but due to their high collision rate with ions the net heat flux is small.

(d) Variation of Energy Deposition with Depth in Target

The main effect is the increased deposition rate as the ions slow near the end of their range (Bragg peak)

$$\frac{dE}{dx} \approx - \frac{E_o/\ell}{2\sqrt{1-x/\ell}} ,$$

where E_o is the initial ion energy and ℓ is its range in cm. This causes factors of 2-3 variation in temperature with depth (x) during the early phase of heating. However, radiation transport smooths the temperature at later times and an effective deposition rate is

$$\frac{dE}{dx} \approx - \frac{E_o}{\ell} ,$$

as assumed in the point model.

(e) Variation of Range with Target Temperature

As the target heats, range shortens (at 75 ev in .05 gm/cm^3 Al it is ~ 60% of the initial value in cold matter)[5]. This behavior is caused by the somewhat greater interaction of the beam with free electrons, which are not as strongly shielded as bound electrons. We ignore this variation since it occurs mainly during the early stages of irradiation (due to a logarithmic dependence of range on free electron density.) The range used here corresponds to $T \approx 75$ eV for the entire pulse.

(f) Disassembly Time

Heated target material expands primarily in the forward direction since a Pb tamper confines it radially and on the back side. There is a corresponding expansion wave which moves into the target at approximately the local speed of sound, C_s.[6] Until this wave reaches the ultimate ion range there is at least a portion of the target which is undisturbed by expansion. We therefore define a disassembly time which is the ion range (in cm) divided by the mean speed of sound during deposition:

$$\tau_d = \frac{\ell}{C_s} = \frac{R/\rho}{\sqrt{\frac{5}{3} \frac{(Z^*+1)\ kT}{M_o}}} . \qquad (2)$$

Here Z^* is the mean ionization state of the target and T is its temperature when heating is 50% complete. M_o is the target particle mass, and ρ is its mass density.

Disassembly times are typically on the order of 10-50 ns, and may be lengthened by decreasing ρ. However, ℓ should not be be allowed to reach a value greater than about twice the beam radius, since irradiance is produced by multiple beamlets covering a significant fraction of a hemisphere. The competition between these criteria strongly drives HTE in the direction of high irradiance. A preliminary study made with LASNEX indicates τ_d is a conservative measure by as much as a factor of two[5] [see also the LASNEX comparisons in Section VIII of this report].

IV. Range

Figure 2 gives the range in Aluminum [200 eV, 0.2 gm/cm^3] for a variety of ions.[7] These curves are a good guide to range in other target materials due to a general insensitivity to atomic type. Particles stopped in Pb have about twice the range they have in Al due in part to the lower electron number per unit mass in Pb and in part to the higher binding energy of core electrons. Note that all ions from Ne to Pb have range close to 10^{-2} gm/cm^2 in Al at 5 MeV/nucleon. As energy increases to 50 MeV/nucleon we have the very rough scaling

$$R \propto E^{1.0} \qquad \text{Pb ions,}$$

$$R \propto E^{1.8} \qquad \text{Ne ions.}$$

This is explained by the fact that Ne is almost completely stripped at 5 MeV/A, while the effective charge of Pb continues to increase with E. In the absence of measurements made in hot dense matter, range is considered to be known to within ± 25% error.

Particle range is only weakly dependent on material temperature and density, so the curves of Fig. 2 should be a fair guide for HTE even though they were derived for application to reactor pellet conditions. Recently a study of range appropriate for HTE has been carried out by R. Kopp using LASNEX[5] (and corroborated at LLNL by J.W-K. Mark). The assumed felt metal is 75 eV Al at .05 gm/cm^3 density. Results are tabulated (Table 1) for several energies and particles and fitted to a power law [$R \propto E^n$ where n depends on particle type]. For Na ions near 100 Mev we have

$$R = \left(.01 \frac{gm}{cm^3}\right)\left(\frac{E}{119\ MeV}\right)^{1.42}, \qquad (3a)$$

and for carbon ions near 50 MeV

$$R = \left(.01 \frac{gm}{cm^2}\right)\left(\frac{E}{51.5\ MeV}\right)^{1.55}. \qquad (3b)$$

A full discussion of range determining factors has been given by Bangerter[8].

V. Specific Energy

Specific energy $\varepsilon(T)$ is not a simple function of temperature. Generally the increase with temperature is more rapid than linear, until

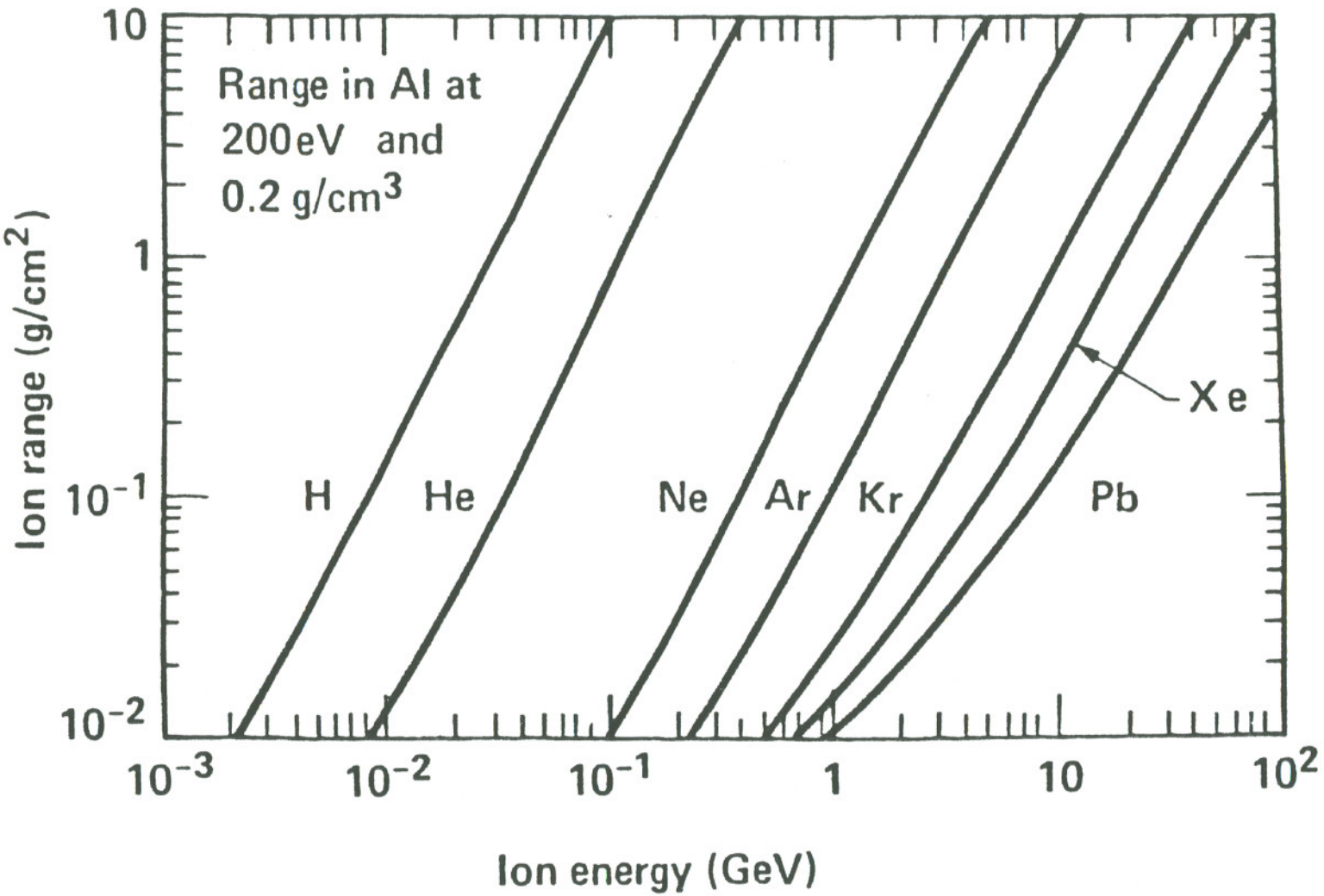

XBL 844-1407

Figure 2. Range-energy plot for ions in hot dense matter

Element (A,Z)	E(MeV) / R(mg/cm^3)	E/R	E/R	$\frac{E}{R}\frac{dR}{dE}$	E for R = 10	Cold Target E for R = 10
Li	7.0	14.0	28.0	1.65	19.9	14.0
(7,3)	2.1	5.6	17.6			
C	18.0	36.0	72.0	1.55	51.5	36.0
(12,6)	2.35	5.73	16.8			
O	27.0	54.0	108.0	1.51	77.5	54.0
(16,8)	2.5	5.8	16.5			
Na	41.5	83.0	166.0	1.42	119.0	83.0
(23,11)	2.7	6.0	16.1			
Si	58.0	116.0	232.0	1.38	162.0	116.0
(28,14)	2.9	6.3	16.4			
A	80.0	160.0	320.0	1.24	226.0	160.0
(40,18)	3.2	6.5	15.4			

Table 1. Ion Range in Al [75 ev, .05 gm/cm^3]. Energy is in units of MeV and range in mg/cm^3. Values in columns 3 and 4 were used to obtain those in 5 and 6 using a power law fit. LASNEX ranges contributed by R. Kopp.

complete ionization is reached. At higher temperatures the increase is linear due to increasing kinetic energy of the components (nuclei and electrons). There is a moderate dependence on atomic type resulting from differences in Z and spacing of ionization levels. There is also a weak dependence on density, which affects the degree of ionization. Experimental data are not readily available for ε at high ρ and T, but some good numerical estimates have been made. The method of Zeldovich and Raisor[9] is applicable if a table of ionization energies is available; a summary is given in Appendix A. Detailed numerical results reported for Aluminum[9] are tabulated here (Table 2). Generally the Zeldovich and Raisor method gives agreement with these to within 10%.

A power law fit to the numerical results obtained for Aluminum yields

$$\varepsilon = (7750 \text{ J/gm})\ T^{1.5}\ \rho^{-.12}\ , \tag{4}$$

with T given in eV and ρ in gm/cm^3. There is no systematic error in the range $10 < T < 150$ and $10^{-2} < \rho < 1.0$, and random errors are on the order of 15%.

The calculation of $\varepsilon(T)$ for Be and Au indicates that high atomic number targets yield a somewhat higher temperature for a given energy deposited; this results from their lower degree of ionization as a fraction of Z at a given temperature. However, for several reasons a high atomic number target is not the preferred choice: the particle range is increased, there may be problems in making a suitable "felt metal", and the Pb tamper will be less effective.

T(eV)	ε (kJ/gm) (Z*) at ρ=.01 gm/cm^3	ε (Z*) at ρ=.1	ε (Z*) at ρ=1.0
10.	351. (2.96)	274. (2.75)	179. (2.29)
20.	1400. (4.44)	953. (3.78)	604. (3.19)
50	6810. (8.53)	4660. (7.01)	2810. (5.50)
80	12000. (10.65)	9180. (9.24)	6280. (7.65)
100.	13800. (10.94)	12000. (10.21)	8590. (8.63)
150.	17200. (11.01)	16400. (10.90)	13900. (10.07)
200.	23400. (11.34)	20300. (11.04)	18400. (10.74)

Table 2. Specific energy ε and ionization Z* for Aluminum

VI. Solution of Heating Equation

We restrict attention to an Al target; from Eq. (4) we have

$$\epsilon = CT^{3/2} , \tag{5}$$

where

$$C = \left(1.02\text{x}10^4 \frac{J}{gm}\right) \left(\frac{\rho}{.1\ gm/cm^3}\right)^{-.12} . \tag{6}$$

Then Eq. (1) becomes

$$\frac{d}{dt} CT^{3/2} = \frac{S-\sigma T^4}{R} . \tag{7}$$

It is assumed that $S(t)$ rises in some specified way from zero to a plateau value S_f, where it is held for the duration of the experiment. The shut-off of $S(t)$ is not considered to be of interest, and is not well treated by Eq. (7), since other factors mentioned in Section III play a large role at late times.

A scale temperature T_f is defined as the final temperature which would be reached at equilibration between irradiation S_f and radiation loss of σT_f^4:

$$T_f = \left(\frac{S_f}{\sigma}\right)^{1/4} = (55.8\ ev) \left(\frac{S_f}{10^{12}\ watts/cm^2}\right)^{1/4} . \tag{8}$$

A second scale quantity is the characteristic radiation cooling rate realized at temperature T_f if S is suddenly turned off:

$$\tau = -\left(\frac{T}{\dot{T}}\right)_f = \frac{3}{2}\frac{RC}{\sigma T_f^{5/2}} \tag{9}$$

$$= (14.9\ \text{ns})\left(\frac{R}{10^{-2}\ \text{gm/cm}^2}\right)\left(\frac{C}{1.02\text{x}10^4}\right)\left(\frac{100\ \text{ev}}{T_f}\right)^{5/2} . \tag{10}$$

We introduce the dimensionless variables

$$x = T/T_f, \quad y = t/\tau\ ; \tag{11}$$

Eq. (7) becomes

$$\sqrt{x}\,\frac{dx}{dy} = \frac{S(y)}{S_f} - x^4 . \tag{12}$$

If $S(y)$ immediately jumps from zero to S_f, then Eq. (12) is separable. The solution is

$$\frac{t}{\tau} = y = \int_0^{T/T_f} \frac{dx\sqrt{x}}{1-x^4} , \tag{13}$$

which is displayed in Fig. 3. Note that in time τ, T reaches 96% of T_f. At early times $T/T_f \approx [(3/2)(t/\tau)]^{2/3}$.

If T has reached T_f and S is suddenly turned off at time t_o, the subsequent decay of T is given by

$$\frac{T}{T_f} = \left(1 + \frac{5}{2}\frac{t-t_o}{\tau}\right)^{-2/5} . \tag{15}$$

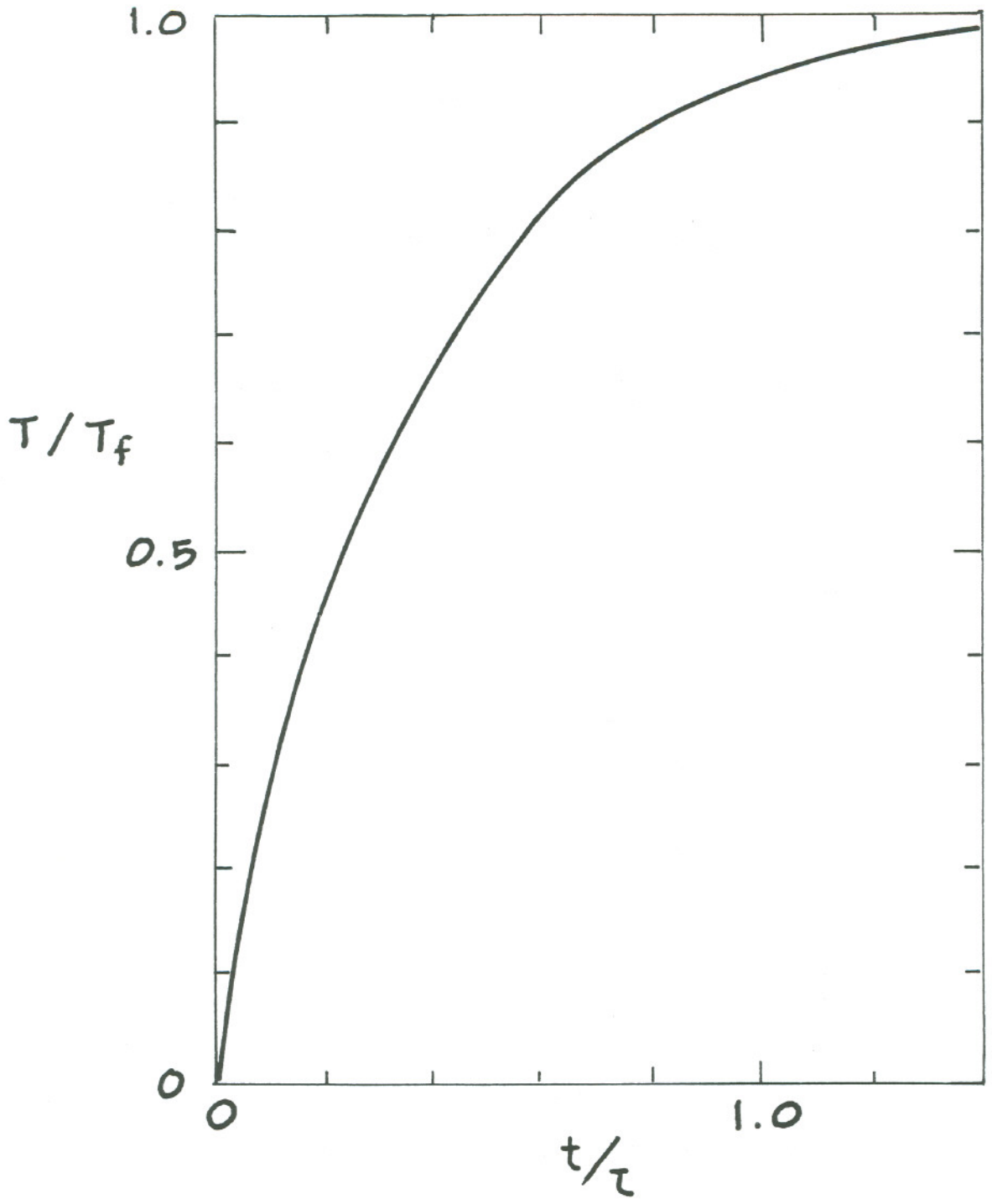

XBL 844-1408

Figure 3. Heating of a disk target by an ion beam. T_f is the asymptotic limit, where radiation loss equals energy deposited per second. The characteristic time τ is defined in text.

In the general case where S rises in non-zero time to S_f, Eq. (12) cannot be separated, and a further approximation is needed to obtain a simple solution. We assume that radiation losses are not important until S has reached its plateau value S_f. [A good HTE design will have a rapid enough rise time.] Then Eq. (1) can be replaced with the simpler (and separable) equation

$$\frac{d\varepsilon}{dt} = \frac{S(t)}{R}\left(1 - \frac{\sigma T^4}{S_f}\right) . \tag{16}$$

For an Al target [$\varepsilon = CT^{3/2}$], and using the dimensionless variables we have

$$\sqrt{x}\,\frac{dx}{dy} = \frac{S(y)}{S_f}\left(1 - x^4\right) , \tag{17}$$

with formal solution

$$\int_0^{t/\tau} dy' \,\frac{S(y')}{S_f} = \int_0^{T/T_f} \frac{dx'\,\sqrt{x'}}{1-x'^4} . \tag{18}$$

The integral on the left of Eq. (18) replaces t/τ when using Figure 3.

VII. Tabulation of Results

In this section we restrict attention to the ideal pulse having zero rise length, so the formulas derived for T_f, τ, and τ_d have a simple interpretation. A large collection of interconnected parameters are available for survey studies, and the procedure adopted here only covers a small set of possible variations. Specifically:

(1) The target is felted Al, with specific energy give by Eq. (5).

(2) Particle type, energy (E), total particle current (I_o), beam edge radius (a), and pulse length (τ_p) are specified.

(3) Beam power (P), pulse energy (W), and irradiance (S_f) are derived from the specified quantities.

(4) Particle range (R) is derived using Eq. (3).

(5) The depth of penetration (ℓ) is set equal to twice the beam radius in order to get the longest disassembly time consistent with a (~30°) angular cone of irradiation.

(6) The target density is derived from the range and depth of penetration.

(7) The "final temperature" (T_f) is derived using Eq. (8).

(8) The radiation scale time (τ) is derived with Eq. (9) [Eq. (6) gives the required value of C.] In time τ the temperature reaches 96% of T_f.

(9) The disassembly time (τ_d) is derived using Eq. (2). Since <u>mean</u> values of Z^* and T during heating should be employed, an approximate τ_d is found by using half the product $(Z^*+1)T_f$.

The pulse length has actually been "postselected" to slightly exceed the radiation scale time, so that the value T_f can be approached. If the disassembly time turns out to be much shorter than the radiation scale time,

then we have a poor choice of parameters. A reduction of radius and proportionate reduction of pulse length is one possible direction of improvement. This may strain focal requirements but it reduces total pulse energy.

Summary of Units

Quantity	Unit	Quantity	Unit
P	TW	R	gm/cm^2
E	MeV	ρ	gm/cm^3
I	A	T_f	eV
W	kJ	τ_p	ns
S	TW/cm^2	τ	ns
a	cm	τ_d	ns
ℓ	cm	Z_f^*	none

Summary of Formulas

$$P = 10^{-6} E I , \tag{19}$$

$$W = P\tau_p , \tag{20}$$

$$S = P/\pi a^2 , \tag{21}$$

$$R = \begin{cases} (.01)(E/119)^{1.42} & (Na^+) \\ (.01)(E/51.5)^{1.55} & (C^+) \end{cases} \tag{22}$$

$$\ell = 2a , \tag{23}$$

$$\rho = R/\ell , \tag{24}$$

$$T_f = (55.8)\, S_f^{.25}\,, \tag{25}$$

$$\tau = (14.9)\left(\frac{R}{.01}\right)\left(\frac{\rho}{.1}\right)^{-.12}\left(\frac{T_f}{100}\right)^{-2.5}\,, \tag{26}$$

$$\tau_d = (\sqrt{2})(\sqrt{27})(788.0)\,\frac{\ell}{\sqrt{T_f(Z^*+1)}}\,. \tag{27}$$

The numerical factor of $(\sqrt{2})$ in Eq. (27) results from using T_f and Z_f^* instead of mean values, and the factor of $(\sqrt{27})$ reflects the mass number of Al (= 27). The value of Z_f^* may be inferred from Table 2.

Results derived for Na^+ and C^+ beams are compiled in Table 3. All cases displayed correspond to plausible HTE parameter sets. The desirability of .05 cm radius rather than .1 cm is obvious, but this will be difficult to achieve due to the smaller required momentum spread at the final lens. Less clear is a choice between C^+ and Na^+. The former would be preferred on the basis of the lower kinetic energy. However, the larger currents required for high irradiance may be very unattractive when the economics of transport are considered.

VIII. Comparison with LASNEX

A spot heating study reported by Mark et al.[3] demonstrates the features of temperature rise and disassembly described in the present report. Their assumed parameters for the most detailed case described are

Table 3. Survey of spot heating predictions

Ion	E	a	T_f	Z_f*	R	ρ	τ	τ_d
	MeV	cm	eV	-	gm/cm^2	gm/cm^3	ns	ns
Na^+	100	.10	70.5	9.5	.00781	.0391	31.2	42.6
Na^+	100	.05	99.7	10.5	.00781	.0782	12.1	17.1
Na^+	150	.10	78.0	10.0	.0139	.0695	40.3	39.5
Na^+	150	.05	110.3	10.2	.0139	.139	15.6	16.5
Na^+	200	.10	83.8	9.4	.0209	.105	48.3	39.2
Na^+	200	.05	118.5	10.4	.0209	.209	18.6	15.8
C^+	50	.10	70.5	9.6	.00955	.0478	37.3	42.4
C^+	50	.05	99.7	10.3	.00955	.0955	14.4	17.3
C^+	75	.10	78.0	9.3	.0179	.0895	50.3	40.9
C^+	75	.05	110.3	10.0	.0179	.179	19.5	16.6
C^+	100	.10	83.8	9.1	.0280	.140	62.3	39.8
C^+	100	.05	118.5	10.3	.0280	.280	24.1	15.8

Table 3 (cont'd)

Ion	Mass	E MeV	a cm	I A	τ_p ns	P TW	S Tw/cm^2	W kJ	ℓ cm
Na^+	(23.0)	100	.10	800	32.0	.080	2.55	2.56	.20
Na^+		100	.05	800	13.0	.080	10.2	1.04	.10
Na^+		150	.10	800	42.0	.120	3.82	5.04	.20
Na^+		150	.05	800	17.0	.120	15.3	2.04	.10
Na^+		200	.10	800	50.0	.160	5.09	8.00	.20
Na^+		200	.05	800	20.0	.160	20.4	3.20	.10
C^+	(12.0)	50	.10	1600	40.0	.080	2.55	3.20	.20
C^+		50	.05	1600	15.0	.080	10.2	1.20	.10
C^+		75	.10	1600	52.0	.120	3.82	6.24	.20
C^+		75	.05	1600	21.0	.120	15.3	2.52	.10
C^+		100	.10	1600	65.0	.160	5.09	10.40	.20
C^+		100	.05	1600	25.0	.160	20.4	4.00	.10

$$E = 100 \text{ MeV } Na^{+}$$

$$a = .017 \text{ cm}$$

$$\rho = .15 \text{ gm/cm}^3 \text{ [Al in a Pb Tamper]}$$

$$P_f = .3 \text{ TW}$$

$$S_f = P_f/\pi a^2 = 330 \text{ TW/cm}^2$$

$$\tau_p = 10 \text{ ns}$$

$$\ell = .1 \text{ cm} .$$

The ion pulse has a 1 ns rise and fall time and a 8 ns flat top, hence W = 2.7 kJ. We denote this run as Case A.

These parameters differ from normally assumed values for HTE primarily in the very small radius (a = .017 cm), which was selected to drive the temperature to over 200 eV. The primary difficulty in achieving such a radius is believed to be the chromatic aberrations of the final focus lens system acting on the expected ±1% momentum spread in the beam.

The computed surface temperature versus time is shown in Fig. 4, reproduced from ref. 3. The peak temperature of 225 eV is reached at 2.3 ns and compares well with the radiation limited value

$$T_f = (55.8 \text{ eV})(330)^{1/4} = 238 \text{ eV} .$$

The latter value is approached very closely (235 eV) at a depth of 0.025 cm. More generally, surface temperature is reported to be ~20% below the peak interior value.

A dramatic fall-off of surface temperature which appears for time greater than 2.3 ns is attributed to disintegration of the surface by hydrodynamic expansion. This behavior can be understood by observing that the

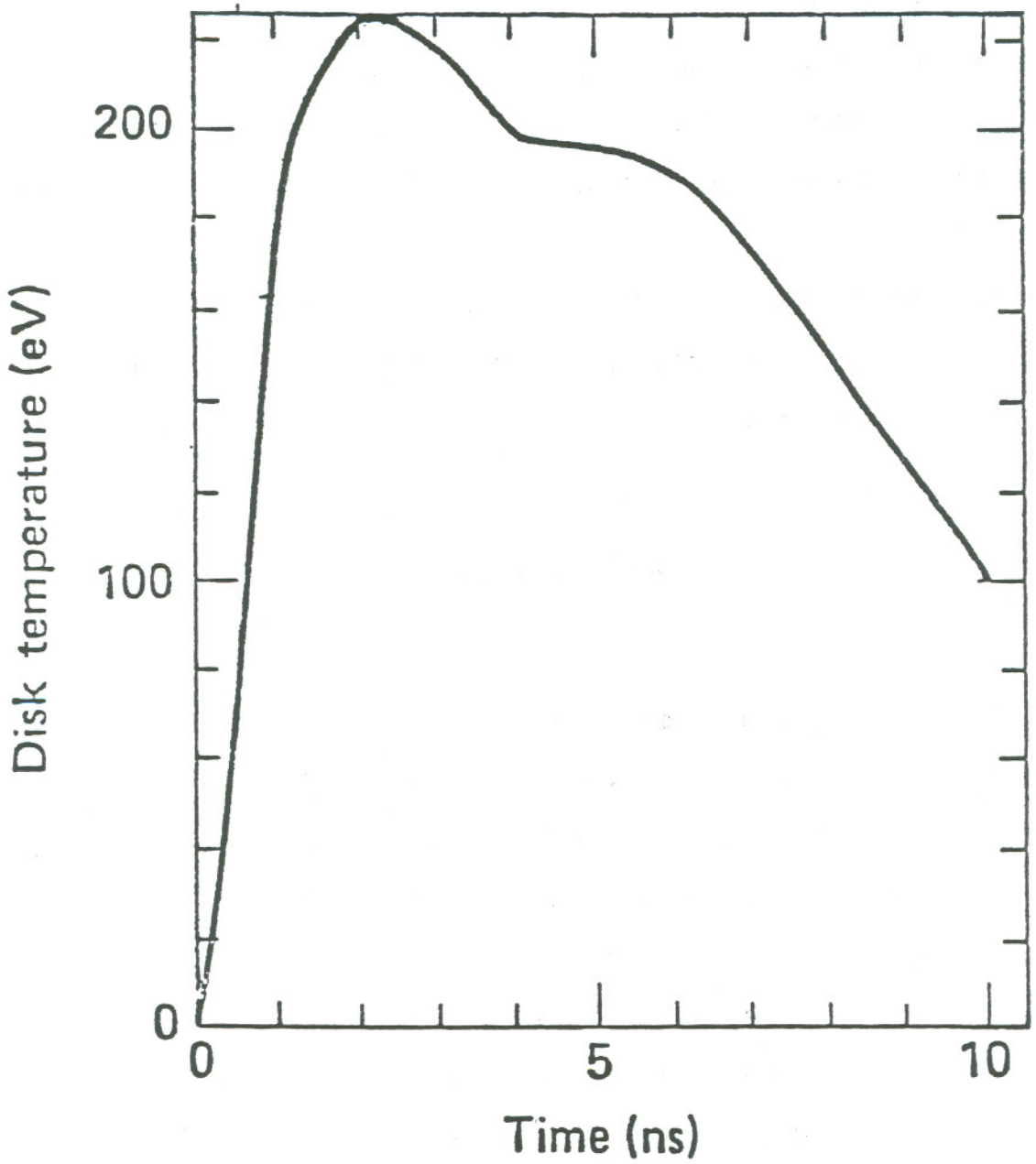

Figure 4. Surface temperature vs. time computed with LASNEX for the spot heating experiment, Case A.

disassembly time for this target is about 5.6 ns. [We use $R = .0078$ gm/cm and $T_f = 238$ eV.] After about 2 ns a .01 cm thickness of Al will be exiting the target but the interior should be relatively undisturbed. This behavior is displayed in a LASNEX zone diagram given by Mark et al.[3] The exiting layer will subsequently expand sideways and receive a much reduced energy deposition from the ion beam. Crudely we expect its temperature to drop on the radiation time scale [Eq. (9)] $\tau \approx 9$ ns, in agreement with Fig. 4.

Another check of the model assumptions is the temperature rise during the first 1 ns, where radiation loss and expansion can be neglected. In $t = 1$ ns the deposited energy is

$$\frac{t}{2}\frac{S_f}{R} = 21000 \text{ kJ/gm} .$$

From the table of specific energies (Table 2), this gives $T \approx 200$ eV, in good agreement with the LASNEX value of ~180 eV (Fig. 4).

In conclusion, the published LASNEX run is an order of magnitude higher in power/cm^2 and half an order smaller in radius than the assumed HTE parameters. However, the results can be quantitatively understood using the model described here, which in fact parallels the discussion of Ref. 8.

We also report here a LASNEX run which is typical of currently assumed parameters for the HTE (such as the 72 eV and 92 eV results of Fig. 7 in Ref. 3). Disassembly of deposition material is more pronounced for the presently considered pulses, which are longer by about a factor of two than those reported in 1982, so that a new simulation is in order. This example has parameters (Case B).

$$E = 125 \text{ MeV } Na^{+}$$

$$a = 0.1 \text{ cm}$$

$$\rho = 0.09 \text{ gm/cm}^3 \text{ [Al in a Pb Tamper]}$$

$$P_f = 0.122 \text{ TW}$$

$$S_f = P_f/\pi a^2 = 3.87 \text{ TW/cm}^2$$

$$\tau_p = 30.9 \text{ ns}$$

$$\ell = 0.2 \text{ cm} \quad \text{[set greater than } R/\rho\text{]} .$$

The ion pulse has a 0.5 ns rise and fall time and a 29.9 ns flat top (Fig. 5), hence $W = 3.7$ kJ. Figure 5 also shows the rate of energy loss from front of disk. Figure 6 gives total energy lost (deposited) as function of time. Figure 7 gives the surface temperature versus time. The initial LASNEX grid is given in Fig. 8 and Fig. 9 gives contour plots of internal temperature in the deposition material at 31 ns. The simulation includes only a small part of the high-Z disk which serves both as mechanical support for and transfer of the low-Z deposition material.

The simple point model predicts for this run

$$R = .0107 \text{ gm/cm}^2$$

$$\ell = R/\rho = .119 \text{ cm}$$

$$T_f = 78.3 \text{ eV}$$

$$\tau = 29.8 \text{ ns}$$

$$\tau_d = 24.7 \text{ ns} .$$

Comparison of these numbers with the LASNEX generated plots reveals several interesting discrepancies. First, the peak LASNEX temperature is about 85 eV, but it follows a broad 80 eV plateau reached after only 12 ns.

These temperatures are significantly higher than those predicted by the simple model at early times. A possible resolution is that shock heating of the emitting zones has occurred. A second point is that disassembly is clearly taking place by the pulse end (see Fig. 9), but it has little effect on the peak temperature.

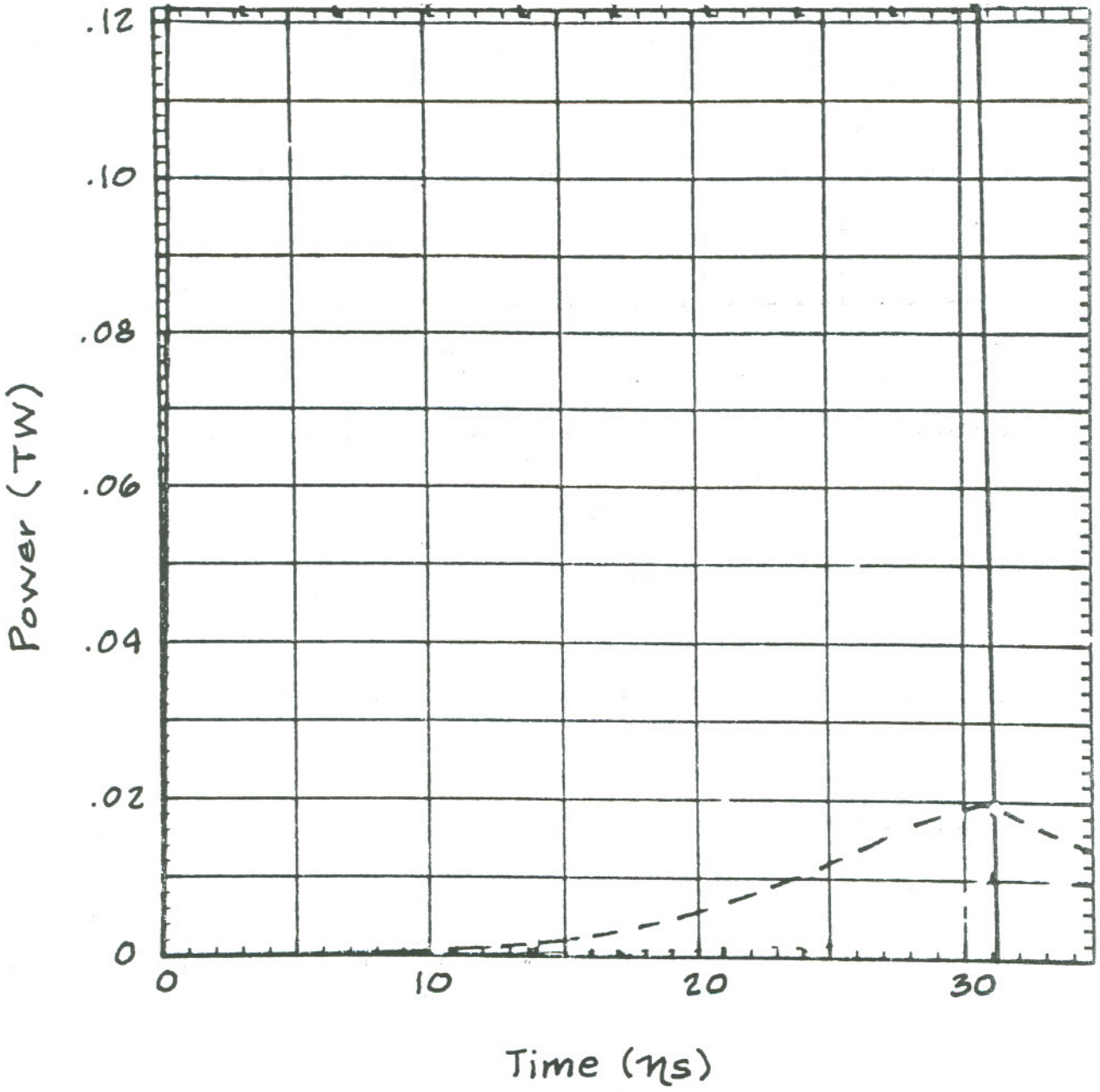

XBL 844-1410

Figure 5. Plot of rate of energy loss from front of disk (dashed curve) versus rate of energy deposition (solid curve) for Case B.

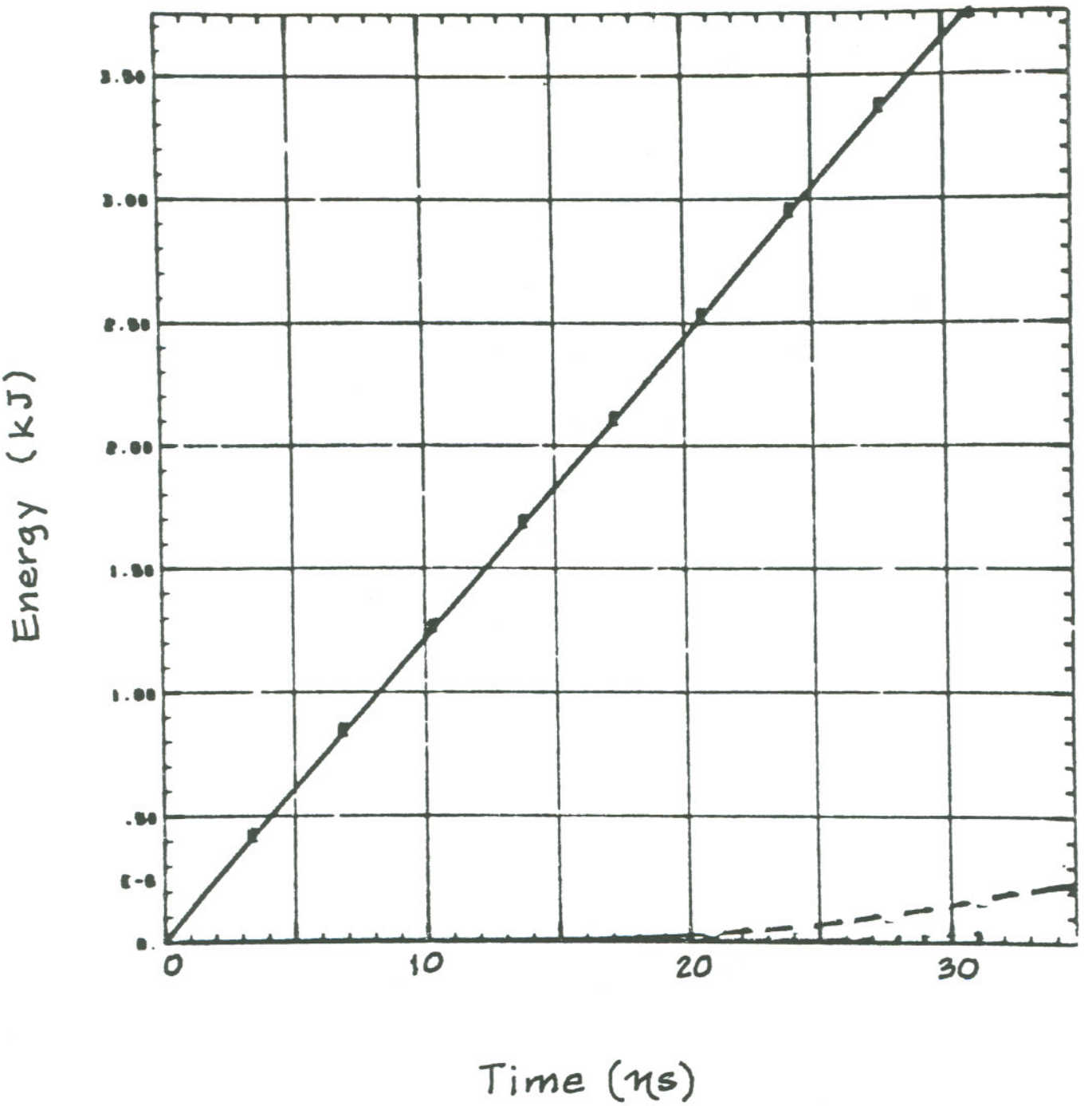

XBL 844-1411

Figure 6. Energy loss for case B. Total energy lost (deposited) is plotted.

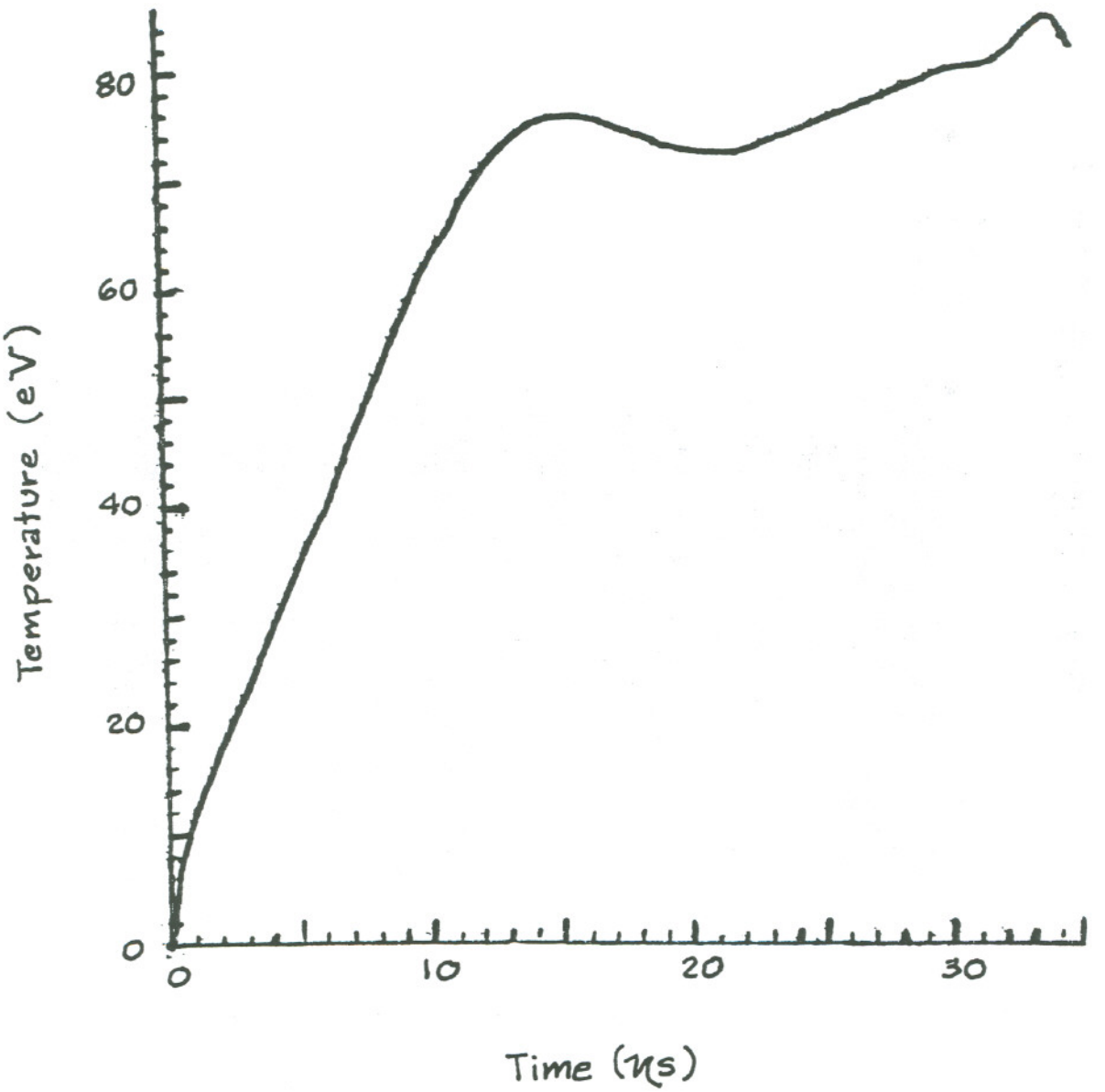

XBL 844-1412

Figure 7. Surface temperature vs. time computed with LASNEX for the spot heating experiment, Case B.

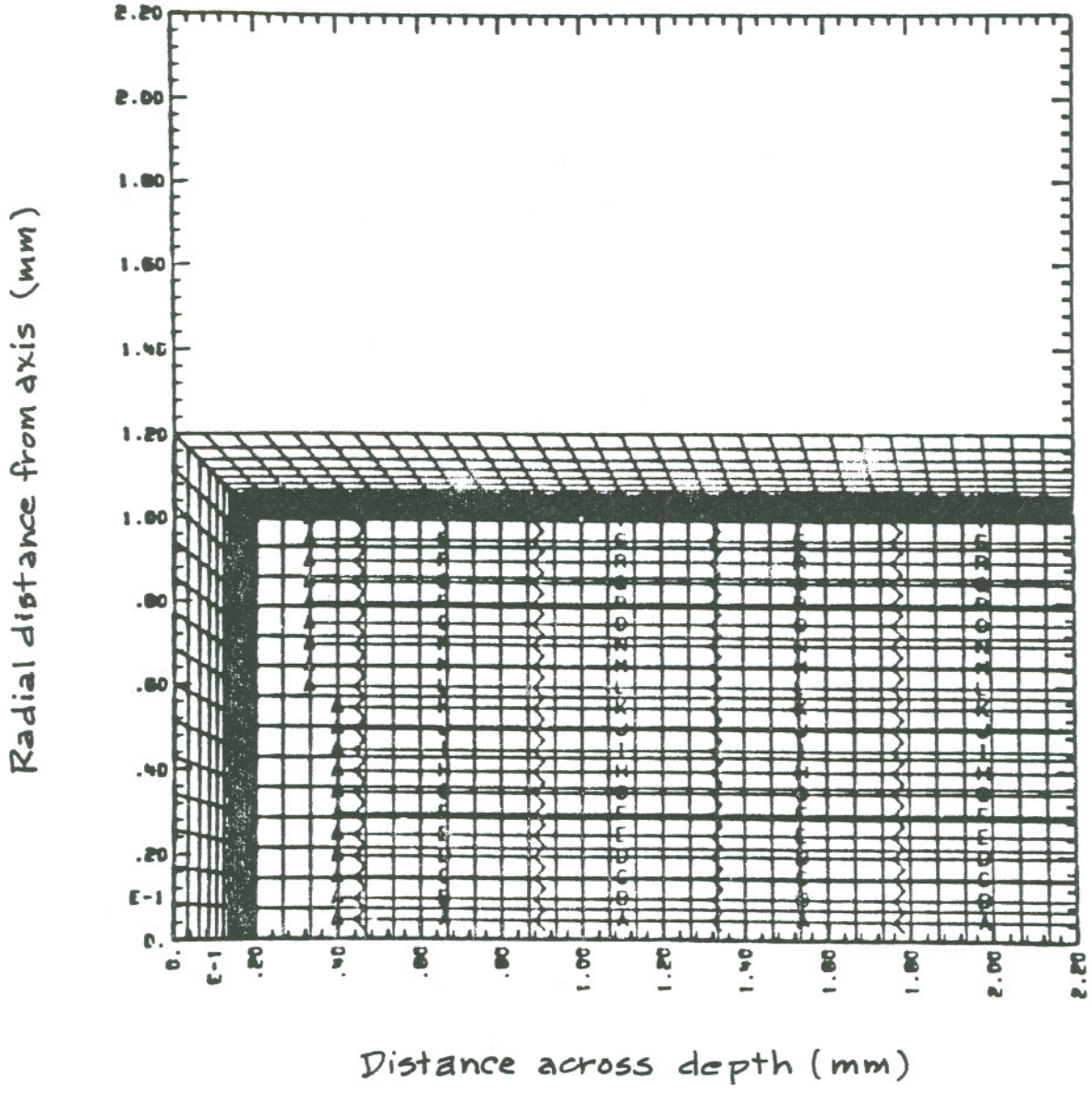

XBL 844-1413

Figure 8. Initial LASNEX numerical grid, Case B.

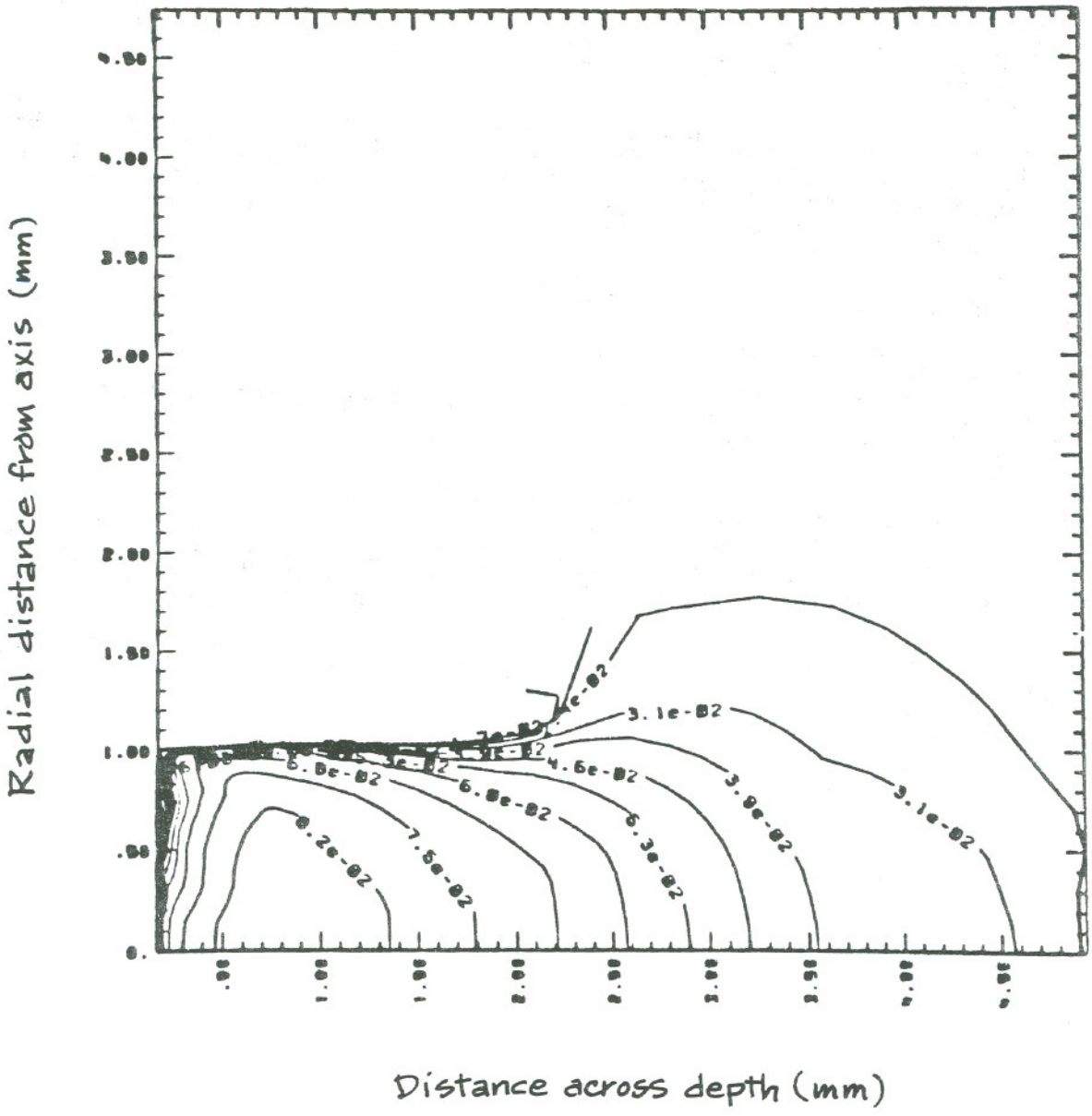

XBL 844-1414

Figure 9. Contour plots of internal temperature in A. Deposition material at 31 ns for Case B.

References

1. Roger O. Bangerter, The U.S. Program in Heavy-Ion Fusion, LA-UR-82:1192, presented at the Symposium on Accelerator Aspects of Heavy-Ion Fusion, Darmstadt, West Germany (April 1982).

2. Heavy Ion Fusion Staff - Lawrence Berkeley Laboratory, A Proposed Program to Develop Linear Induction Accelerator Technology in Support of the National Accelerator Inertial Fusion Plan, LBL PUB-5065, February 1982.

3. J. W.-K. Mark et al., Heavy-Ion Inertial Fusion: Suggested Experiments on Disk Heating and Beam Transport Using Accelerator Test Facilities, Proceedings of High-Power Beams 81, H.J. Doucet and J.M. Buzzi, Editors, Ecole Polytechnique, Palaiseau, France, 1981, pg. 649.

4. Roger O. Bangerter, Private communication.

5. R. Kopp, Private communication.

6. J. Bond, K. Watson and J. Welch; Atomic Theory of Gas Dynamics, Addison-Wesley, 1965, pg. 64.

7. D. Keefe, Ann. Rev. Nucl. Part. Sci., 1982, 32, pg. 429.

8. Roger O. Bangerter, Ion Beam Interactions With ICF Targets, Proceedings of the Sixth International Workshop on Laser Interactions and Related Plasma Phenomena, held in Monterey, Ca., Oct. 25-29, 1982.

9. R.J. Harach and F.J. Rogers, J. Appl. Phys., Vol. 52. No. 9, Sept. 1981, pg. 5594.

10. Allen, Astrophysical Quantity, 3rd Ed., 1973, pg. 37.

APPENDIX A

The Method of Zeldovich and Raisor[9]

Specific energy is assumed to be adequately given by the sum of the mean ionization energy of heated matter, and the kinetic energy of its constituents (electrons, atoms and ions). This is

$$\varepsilon = N\left[Q\,(\bar{Z}^*) + \frac{3}{2}\,(1+\bar{Z}^*)kT\right] , \qquad (A\text{-}1)$$

$$N = 6.02 \times 10^{23}/A_T , \qquad (A\text{-}2)$$

where N is the number of heavy particles per gram (target atoms and ions of atomic number A_T), Z^* is their mean ionization level, and $Q(Z^*)$ is the energy required to reach Z^*. The ionization energies I, $I_2, \ldots I_z$ are assumed to be known [see Allen (Ref. 10) for first 10 levels]. Then

$$Q(Z^*) = I_1 + I_2 + \ldots + I_{Z^*} . \qquad (A\text{-}3)$$

The mean Z^* is determined by the solution of Saha's equation:

$$I\left(\bar{Z}^* + \frac{1}{2}\right) = kT\ \ell n\left[\frac{10^{-2} A_T (kT)^{3/2}}{\bar{Z}^*\ \rho}\right] \qquad (A\text{-}4)$$

with kT in eV and ρ in gm/cm^3. The ionization energy I at fractional values of $(\bar{Z}^* + 1/2)$ is determined by interpolation. Equations (A-1) through (A-4) are easily solved with a standard root finding routine.